Nonresonant Raman Imaging of Protein Distribution in Single Human Cells

N. UZUNBAJAKAVA,[1] A. LENFERINK,[1] Y. KRAAN,[1] B. WILLEKENS,[2] G. VRENSEN,[3] J. GREVE,[1] C. OTTO[1]

[1] Biomedical Technology Institute, Department of Applied Physics, University of Twente, P.O. Box 217, 7500 AE Enschede, The Netherlands

[2] The Netherlands Ophthalmic Research Institute, P.O. Box 12141, 1100 AC Amsterdam, The Netherlands

[3] Department of Ophthalmology, Leiden University Medical Center, P.O. Box 9600, 2300 RC Leiden, The Netherlands

Received 25 March 2002; revised 7 May 2002; accepted 16 May 2002

ABSTRACT: A confocal Raman microscope is used to study the protein distribution inside biological cells. It is shown that high quality Raman imaging of the protein distribution can be obtained using confocal nonresonant Raman imaging (λ_{exc} = 647.1 nm). The results are shown for two different human cell types. Perpheral blood lymphocytes are used as an example of the fully maturated cells with a low level of nuclear transcription. Human eye lens epithelial cells are used as an example of cells with a high level of nuclear activity. The protein distribution in both cell types is completely different. The nuclear distribution of the protein largely varies in the peripheral blood lymphocyte cells, while proteins are more homogenously distributed over the nuclear space in the eye lens epithelial cells. The imaging time is ~20 min for a field of view of 10×10 μm^2. The size of the sampling volume is 1.4 fL using a full width at half-maximum criterion along the z axis and a $1/e^2$ criterion in the xy plane. The results presented here indicate that Raman imaging is particularly of interest in the study of cellular processes, like phagocytosis, apoptosis, chromatin compaction, and cellular differentiation, which are accompanied by relatively large-scale redistributions of the materials. © 2002 Wiley Periodicals, Inc. Biopolymers (Biospectroscopy) 72: 1–9, 2003

Keywords: nonresonance Raman imaging; confocal Raman imaging; single cell; protein distribution; nuclear organization; transcription level

INTRODUCTION

Cellular processes, such as mitosis, apoptosis, and phagocytosis, are accompanied by large material redistributions on the scale of the dimensions of the cell, which is typically on the order of 10s of microns. Imaging the distribution and changes in the distribution of the molecules that make up the cell is an important way to learn about cellular processes that underly the molecular make-up and distribution. Different materials contain different molecular bonds. This gives rise to a different vibrational spectrum. IR microscopy[1] and Raman microscopy (spontaneous Raman scattering as well as coherent anti-Stokes Raman scattering (CARS)[2]) utilize this chemical specificity to generate a contrast within an image. In contrast with IR microscopy, which is based on light absorption,[1] images in CARS[2] and spontaneous Raman microscopy are generated through

Correspondence to: N. Uzunbajakava (n.uzunbajakava@tn.utwente.nl).

Biopolymers (Biospectroscopy), Vol. 72, 1–9 (2003)

light scattering. None of these techniques require any staining procedure.

In order to visualize the protein distribution in cells, we improved the sensitivity of a lab-built confocal Raman microscope so that nonresonant Raman scattering can be utilized as the contrast generating scattering process. Raman images were previously obtained from lymphocytes using preresonant Raman scattering from carotenoids[3] and red blood cells[4] by utilizing the resonant Raman scattering from hemoglobin. In addition, the lipid and cholesterol distributions inside the lens fiber cells were studied by using Raman microspectroscopy and imaging.[5,6] The Raman microscope has also been successfully applied to the study of drug distributions inside cells.[7,8] Resonant Raman microspectroscopy has also been used to study eosinophyl peroxidase in eosinophilic granulocytes[9] and NADPH oxidase and myeloperoxidase in neutrophilic granulocytes.[10] The temporal changes in the redox state of the enzymes in these leukocytes could also be followed in vivo using resonant Raman scattering.[11]

Nonresonant Raman scattering is 3–4 orders of magnitude weaker than resonant Raman scattering. In this study we show the feasibility of nonresonant Raman imaging of the protein distribution in cells for the first time. To achieve this we improved an available Raman microscope. In principle, improvements are found in a combination of the following technical aspects: an increase of the laser power, an increase in the measurement time, and an increase in the total sensitivity of the Raman microscope. In general, it can be said that nonresonant Raman scattering demands high concentrations of material. This criterion is automatically fulfilled for the proteins and DNA in the extremely condensed space within a biological cell, in which the DNA concentration may be as high as 100 mg/mL, the protein concentration is 250 mg/mL, and the RNA concentration is 100 mg/mL, depending on the cell type, the phase of the cell cycle, and the location inside the cell.[12] Our further aim is to obtain the protein distribution at a spatial resolution that is as high as possible. For this we employ the confocal measurement principle in combination with Raman microscopy.

In this study we compare Raman images of two cell types, peripheral blood lymphocytes (PBLs) and eye lens epithelial cells (LECs). Mature PBLs are chosen because they are terminally differentiated cells. In these cells transcriptional activity is low and no replication takes place under physiological conditions.[13] On the other hand, LECs are metabolically active cells. They are primary responsible for eye lens growth, maintenance of its homeostasis, and detoxification of noxious components in the environment throughout its life.[14] LECs are further involved in the synthesis of both lens-specific and common cell proteins.[14] Thus, transcription in the epithelial cells is at the level required to sustain these processes and replication may occur. Among the active cells, LECs were of interest because of the possible relation between controlled cell death (apoptosis) and the occurrence of cataractous changes.[15,16] These results will be presented in a future article.

MATERIALS AND METHODS

The peripheral blood of healthy donors was obtained by venipuncture and collected in heparinized tubes. The PBLs were isolated using standard density centrifugation followed by monocyte depletion. The sample contains T, B, and K cells and represents a monolayer of round cells adhered to the surface of a substrate and separated from each other by a distance of about 20 μm.

Human donor eye lenses, which were extracted within 24 h postmortem, were obtained from the Cornea Bank of Amsterdam (The Netherlands Ophthalmic Research Institute, Amsterdam). Ex in vivo cataract surgery was performed, including posterior capsulorhexis, hydroexpression of lens fiber mass using Eagle's minimal essential medium supplemented with 2% fetal calf serum, and aspiration of residual fibers. The capsular bag was then dissected. Subsequently, the capsular bag, consisting of the anterior capsule and the monolayer of LECs, was flat mounted on a calcium fluoride (CaF_2) substrate (Spectroscopy Central Ltd.) and fixed with 2% paraformaldehyde.

The LEC and PBL cells were deposited on a CaF_2 substrate. This material contributes a relatively low background compared to glasses (microscope slides or quartz, data not shown). The CaF_2 disks were incubated overnight in a solution of 0.01% poly-L-lysine (PLL, P-1274, Sigma) in phosphate-buffered saline (PBS) at 4°C. A few drops of the PBL suspension in RPMI 1640 medium without phenol red (Gibco) were added onto a PLL-coated CaF_2 substrate to form a distribution of single cells. After incubation at 37°C for 30 min the adhered PBLs were fixed in 1% paraformaldehyde.

The fixed PBLs and LECs were washed 3 times in PBS. A CaF_2 disk containing cells or capsular bags was transferred to a petri dish (3.5-cm diameter) and 3 mL of PBS was added.

Confocal Raman Microspectrometer

All Raman measurements were done with a lab-built confocal Raman microspectrometer.[17] The excitation wavelength was the 647.1-nm line from a Kr ion laser. Raman images were collected in the following way. During Raman imaging a full spectrum ($\sim$1800 cm^{-1} width) of each position of the laser beam inside the cell was recorded. Raman images of a single cell in any vibrational band of interest were reconstructed after the measurement. The sample was scanned in steps of 130–190 nm. In this way the sampling interval was 2–3 times smaller than the diffraction-limited laser spot on the sample, which approximates the Nyquist theorem. The field of view is approximately 58 μm in diameter when a 63$\times$ NA = 1.2 water immersion objective (Zeiss Plan Neofluar) is used. A blazed holographic grating with 600 grates/mm (Jobin–Yvon, Paris) was used for dispersion; the spectral resolution on the charge coupled device camera (CCD) was 1.7 cm^{-1}/pixel. The lateral resolution is limited by the diffraction and is 550 nm for our system. The definition of the resolution is based on the diameter of the laser beam waist at which the beam intensity has fallen to $1/e^2$ of its peak value.

Power Dependency Measurements

High laser powers are often used in nonresonant Raman experiments. We thoroughly investigated how much laser power and for what period of time it could be used without causing a change in the Raman spectrum of the single cells. Experiments were performed on fixed PBLs in a physiological buffer (PBS). Ten Raman spectra were acquired from a single point inside the cell nucleus, each for a period of 10 s. This procedure was performed for six different powers in the range from 10 to 140 mW, and it was repeated each time for 10 cells.

The sets of 10 spectra for each measured cell were analyzed using the method of singular value decomposition. This analysis showed that up to 70 mW of laser power for up to 100 s does not induce a change in the Raman spectrum of a single cell.

Axial Resolution

In the confocal measurements the microscope objective forms a diffraction-limited image of the laser beam in the object. An image of the illuminated spot is formed at the position of the field stop. In our setup we use a circular pinhole to reject out of focus light and to set the desired confocal resolution. Thus, the axial resolution and signal intensity passed through the field stop would directly depend on the chosen pinhole size. Gaussian beam theory was used to estimate the 3-dimensional resolution of our confocal Raman microscope.[18] In these calculations the beam was traced from the focus in the laser resonator through each lens in the setup through the water-immersion microscope objective and back to the pinhole. Simulation of a z scan of a thin slice through the focus and calculation of the intensity of the Raman shifted frequency (1002 cm^{-1} of toluene) through the pinhole provides a prediction of the axial resolution. The full width at half-maximum (FWHM) of the intensity profile was used as a criterion for the axial resolution. This "soft" criterion leads to a resolution that is worse than that based on, for instance, the Rayleigh criterion. Furthermore, it is experimentally based on measurements on thin, planar objects, which will always lead to an underestimation of the resolution with which small spherical objects can be measured. First a pinhole of 50 μm was used as a field stop, giving a 5-μm axial resolution on a basis of the FWHM criterion. This was not sufficient to easily discriminate between nuclear and other contributions within a multilayer complex sample, such as LECs. LECs are $\sim$12 μm high with a nucleus diameter of $\sim$8 μm. Gaussian beam theory predicts that the axial resolution is increased to 2.4 μm when a 25-μm diameter pinhole is used. This prediction was confirmed by the experimental determination of the resolution in axial scans of a thin polystyrene layer on silica substrate. The total measurement volume in the microscope was decreased to 1.4 fL, again using a FWHM criterion in the axial direction and the size of the laser beam waist in the lateral direction.

RESULTS AND DISCUSSION

The effect of two different pinhole sizes (50 and 25 μm) on the Raman spectrum is illustrated in spectrum A in Figure 1. The nonresonant Raman

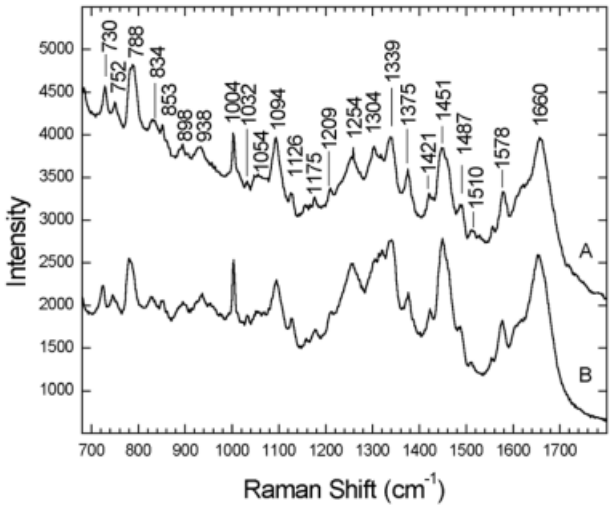

Figure 1. Raman spectra of living PBL nuclei measured with different sizes of confocal pinholes: (A) 50-μm diameter confocal pinhole; the spectrum represents an average of measurements on seven cell nuclei; (B) 25-μm diameter confocal pinhole; the spectrum represents an average of measurements on two cell nuclei. PBLs were adhered to CaF_2. All measurements were done in PBS as the physiological buffer. The laser power was 30 mW, and the accumulation time was 100 s. The Raman line assignments are detailed in Table I.

spectra were measured from the nucleus of single living PBL cells in PBS as described in the Materials and Methods. Raman spectra were acquired during 100 s with 30-mW laser power on the sample.

The spectrum represents an average of measurements on seven cell nuclei. The Raman spectrum of the PBL nucleus is in agreement with Raman spectra of the same cells that were obtained earlier using a 660-nm excitation wavelength.[19] The assignment of the vibrational bands can be made on the basis of literature data.[20,21] The Raman spectrum contains bands that are typical for polynucleotides and proteins. The Raman peak assignment is presented in Table I.

In spectrum B in Figure 1 the Raman spectrum of a PBL nucleus is presented using a pinhole of 25 μm. A comparison of spectra A and B in Figure 1 shows that the smaller pinhole size leads to a reduction in the contribution of the background (water) spectrum by a factor of 2. This is also in agreement with a prediction on the basis of Gaussian beam theory.

The effect of increased confocal resolution can also be obtained from the axial scans of the human LEC. In Figure 2 we show typical spectra obtained at different depths in the sample. The gradual changes from a Raman spectrum typical for the cytoplasm (Fig. 2, upper part, spectrum A) to that for the nucleus (Fig. 2, intermediate part, spectra C–E) to that for the capsular bag (Fig. 2, lowest part, spectrum H) are clear.

It is well known that biological macromolecules are not homogeneously distributed inside the cell. The distribution of molecules is related to their very localized and specific activity. In spectra A and B in Figure 3 we show Raman spectra of different locations in the same nucleus of PBLs. Data were accumulated over 100 s using 30 mW of laser power under the objective. The analysis of

Table I. Raman Line Assignments for Lymphocyte Nucleus

Peak Position (cm^{-1})	Assignment[16]
730	A ring breathing
752	T ring breathing
783, 788, 792	C ring breathing, T; n: bk: O–P–O sym. str.
834	n: RP, Tyr
853	Tyr
898	n: bk; p: C–C skeletal modes
938	p: α helix; p: C–C skeletal modes
1004	Phe; p: C–C skeletal modes
1032	Phe; p: C–N str.
1054	n: CO str.; p: C–N str.
1094	n: bk: O–P–O sym. str.; p: C–N str.
1126	p: C–N str.; p: C–N str.
1175	Tyr, Phe;
1209	Phe, Tyr; p: amide III
1254	A; p: amide III
1304	A; p: amide III
1339	A
1375	T, A, G
1421	A, G
1451	CH def.
1487	G, A
1510	A
1578	G, A
1660	p: amide I
2850	CH_2 sym. str.
2885	CH_2 asym. str.
2935	CH str.

Phe, phenylalanine; Tyr, tyrosine; p, protein; n, nucleotide; A, adenine; T, thymine; G, guanine; C, cytosine; sym., symmetric; asym., asymmetric; str., stretching; def., deformation; bk, backbone.

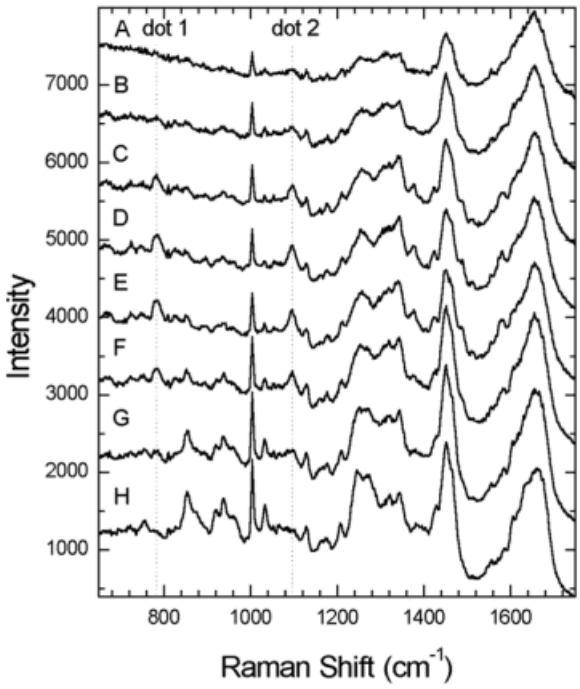

Figure 2. A scan through the nucleus of the fixed LEC. The axial displacement was 1 μm. In spectra A–H the scanning is from the top of the cell to the capsular bag. Dot 1 indicates the 788 cm^{-1} band; dot 2 is the 1094 cm^{-1} band. The laser power was 30 mW, and the accumulation time was 100 s. A 25-μm diameter confocal pinhole was used. The Raman spectra are shifted along the intensity axis for clarity.

the spectral data from different PBL nuclei (data not shown) shows that the DNA and protein signals are not of the same intensity throughout the nucleus. Moreover, the DNA/protein intensity ratio also varies within a factor of 30% of the average ratio. This variation is quite large, especially if it is taken into account that the size of the volume from which the Raman spectrum is acquired is still quite large and it must be supposed that a considerable amount of spatial averaging is still in place.

The Raman spectra of the epithelial cell nucleus (Fig. 3, spectrum C) show a number of differences with respect to those of the PBL cells. First, the DNA signal (788 and 1094 cm^{-1} bands) is much lower in the epithelial cell than in the nucleus of the PBL cell. Second, the Raman intensity from protein (1449 cm^{-1}) is relatively large for the epithelial cell. A direct consequence of these observations is that the DNA/protein intensity ratio is considerably higher in the LECs than in the PBL cells.

A complete and detailed interpretation of the distribution and organization of the chromatin depends on numerous parameters: the cellular type, proliferation activity, differentiation, transcription, and metabolism must all be considered.[22,23] However, consideration of the size of the nuclei and the metabolic state will give a preliminary qualitative understanding of the differences that are observed in the Raman spectra of the PBL and LEC nuclei. The nuclei of the small PBLs have a diameter of about 6 μm,[24] while the nuclei of the LECs are about 8 μm (our TEM data). The LECs and PBLs are both human. They contain the same amount of DNA (approximately 6×10^9 base pairs) distributed inside the cell nuclei. A difference in the diameter of the nucleus will strongly affect the concentration of DNA. The second factor to take into account is the chromatin compactness and the metabolic state of the cell. A mature lymphocyte sustains only a low level of transcription and, being mature, will not replicate its DNA any further. TEM studies revealed that the nucleus of mature lymphocytes shows large domains of highly condensed and inactive heterochromatin.[25] Naturally, a high DNA and protein concentration can thus be expected in areas of the lymphocyte nucleus. This is directly evidenced in the Raman spectra. The epithelial

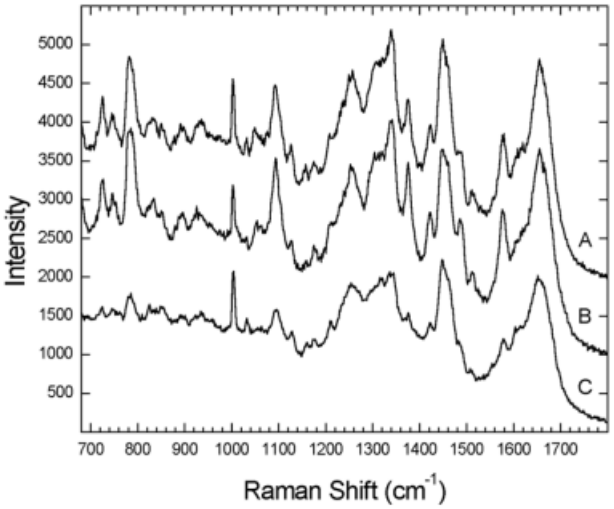

Figure 3. Raman spectra of the nuclei of different cell types measured in a nucleus of fixed PBL (spectra A and B) and measured in a nucleus of fixed LEC (spectrum C). All cells were adhered to CaF_2. The laser power was 30 mW, and the accumulation time was 100 s with a 25-μm diameter confocal pinhole. The Raman spectra are shifted along the intensity axis for clarity.

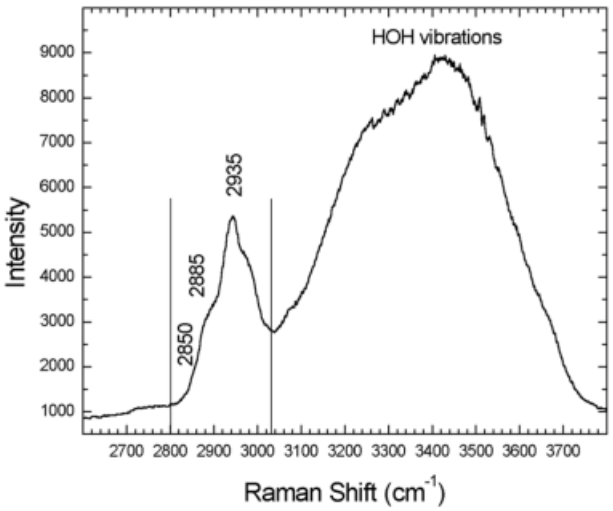

Figure 4. The high frequency Raman spectrum of the PBL nucleus (average of measurements on six fixed cells). The PBLs were adhered to CaF_2. All measurements were done in a physiological buffer. The laser power was 30 mW, and the accumulation time was 60 s with a 25-μm diameter confocal pinhole. For Raman imaging the spectral region between two lines was used.

cells, however, are involved in the maintenance of the eye lens metabolism and development. This task requires a large amount of transcriptive and, in the case of cell division, replicative activity. These processes require some decondensation of the chromatin structure and the presence of all proteins to sustain biomolecular synthesis, such as the repair of proteins, replication factors, RNA polymerase, and so forth. These two factors, namely, the size of the cell nucleus and the level of transcription, agree with our observation that lower DNA intensities (788 and 1094 cm^{-1} bands) are measured in the Raman spectrum of the nucleus of the LEC in comparison to that of the PBL cell. Also in agreement with this line of thinking is the observation that the protein intensity (1449 cm^{-1} bands) in epithelial cells is high in comparison with that in PBL cells. This makes the total DNA/protein ratio in epithelial cells higher than in lymphocytes.

In order to test this observation further, Raman images were made of the protein distribution using the high frequency region of the Raman spectrum of the cells (Fig. 4). In this spectral region the alkane groups of the proteins contribute strong CH stretch vibrations at 2850 (symmetric CH_2 stretch), 2885 (asymmetric CH_2 stretch), and 2935 cm^{-1} (CH stretch). More minor contributions from CH stretch modes in DNA also occur. At around 3400 cm^{-1} the Raman scattering from the O—H stretch vibration from water gives a very strong contribution to the Raman spectrum.

Although the chromatin distribution in lymphocytes and LECs was analyzed by TEM and the chromatin compactness was studied by the fluorescence method, no information was obtained thus far on the single cell level without using specific stains or labels.

The Raman image of a fixed PBL cell in a physiological buffer on a CaF_2 substrate is shown in Figure 5(A). The spectral data were acquired by scanning an 8×8 μm area with a 1-s accumulation time per step and a laser power of 120 mW. The step size was 127 nm. The Raman image was constructed from the whole band from 2800 to 3030 cm^{-1}, which is shown as the arched area in Figure 4. The bias offset of the CCD camera was subtracted, but minor contributions of the water signal are still present in the image. Two line profiles of the protein distribution in the lymphocyte nucleus are shown in Figure 5(B). The transmission bright light image of a cell [Fig. 5(C)] was made with a video camera implemented into the setup.

The protein Raman image of the PBL [Fig. 5(A)] shows the presence of considerable variations in the protein signal. The two line profiles, corresponding to lines a and b through the image, show that protein intensity changes up to 8% of the average signal in the cell nucleus occur. Also, the spatial size of the regions with high and low protein intensities can be as large as ~ 1 μm.

The signal-to-noise ratio (data not shown) is high enough to distinguish differences in the signal with 2% accuracy, even in the regions with the lowest protein signal (i.e., in the cell cytosol of PBL). Hence, the noise level is considerably lower than the intensity variations in the Raman images of the protein distribution.

In the bright light image of the PBL cell [Fig. 5(C)] we can clearly distinguish the cell cytosol, which is less then 1 μ in the lateral dimension. The nucleus occupies the largest part of the cell volume.

A Raman image of the fixed LEC in a physiological buffer on CaF_2 substrate is given in Figure 6(A). The line profiles through the image are shown in Figure 6(B) and the bright light view of a cell is in Figure 6(C). The epithelial cell contains a cytoplasmic region that, unlike from the PBL cell, contains a considerable part of the cellular volume. The cell nucleus can be clearly distin-

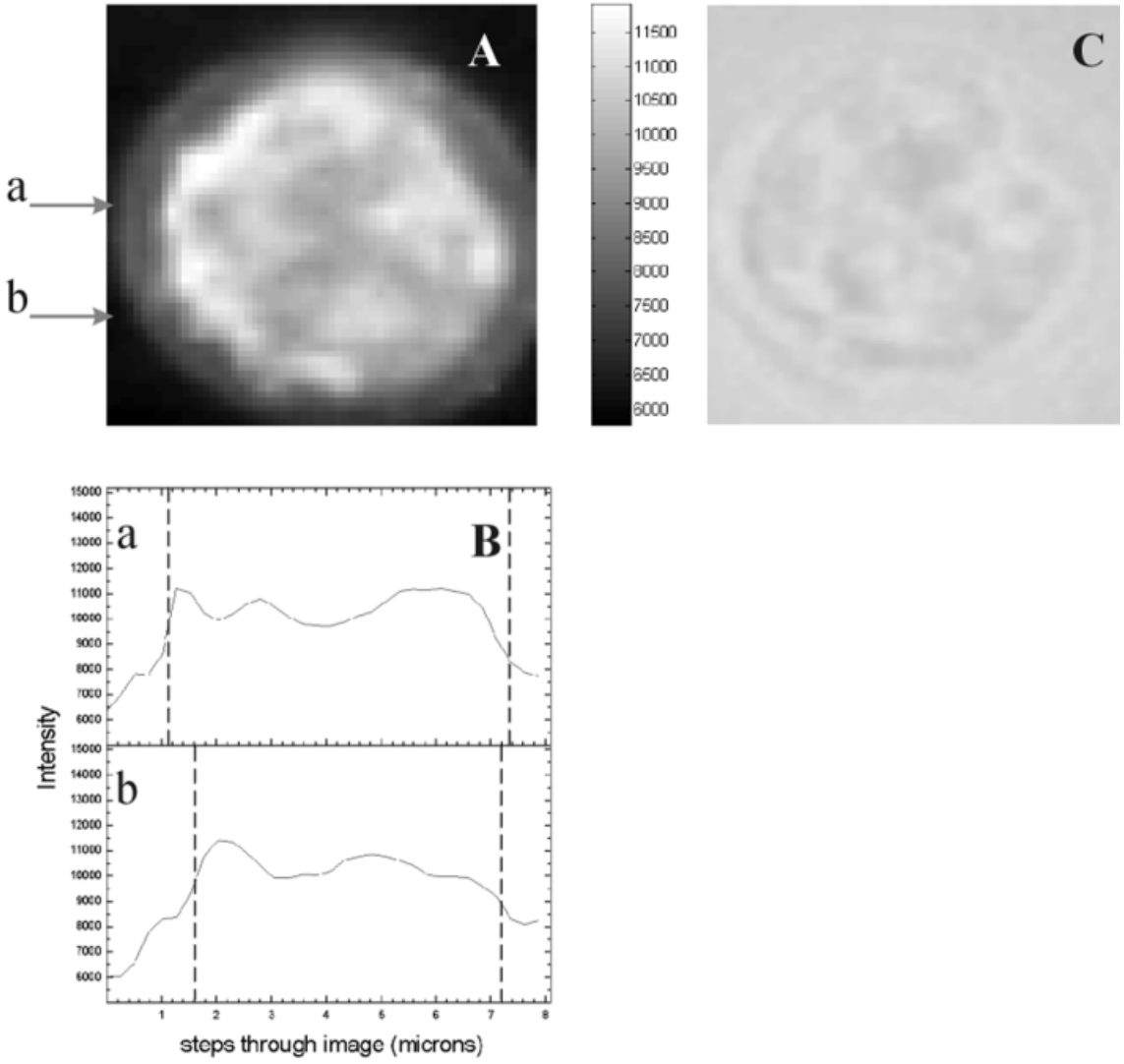

Figure 5. Raman imaging of a single fixed PBL in physiological buffer. (A) Raman image made in a high frequency protein band consisting of 2850 cm^{-1} symmetric CH_2, 2885 cm^{-1} asymmetric CH_2, and 2935 cm^{-1} CH vibration modes; (B) two profiles through the protein image corresponding to lines a and b; (C) a transmission bright light image of a PBL. The scanning area was 8 × 8 μm. The laser power was 120 mW, and the acquisition time was 1 s/step.

guished from the surrounding cytosolic region [Fig. 6(C)].

The Raman image of the fixed epithelial cell in a physiological buffer [Fig. 6(A)] was acquired with a 1-s accumulation time and 60 mW of laser power on the sample. An area of ~12 × 12 μm was scanned with a sampling interval of 188 nm.

A striking feature in the Raman image of the epithelial cell is the homogeneity of the protein distribution inside the nucleus on a submicron scale. Both line profiles made through the epithelial cell nucleus [Fig. 6(B)] show that the dramatic intensity variations occurring in the PBL cells [compare Fig. 5(B)] are absent in the epithelial cell. The signal-to-noise ratio (data not shown) shows that we are able to detect protein intensity variations with an accuracy of about 3.5%.

Another difference between these two cells appears from a comparison of the protein images. The protein intensity in the cytoplasm of the epithelial cell is much higher than in the cell nucleus. In the PBL cell an inverse relationship is observed. The spectroscopic measurements also confirmed a higher protein signal in the cytosol of

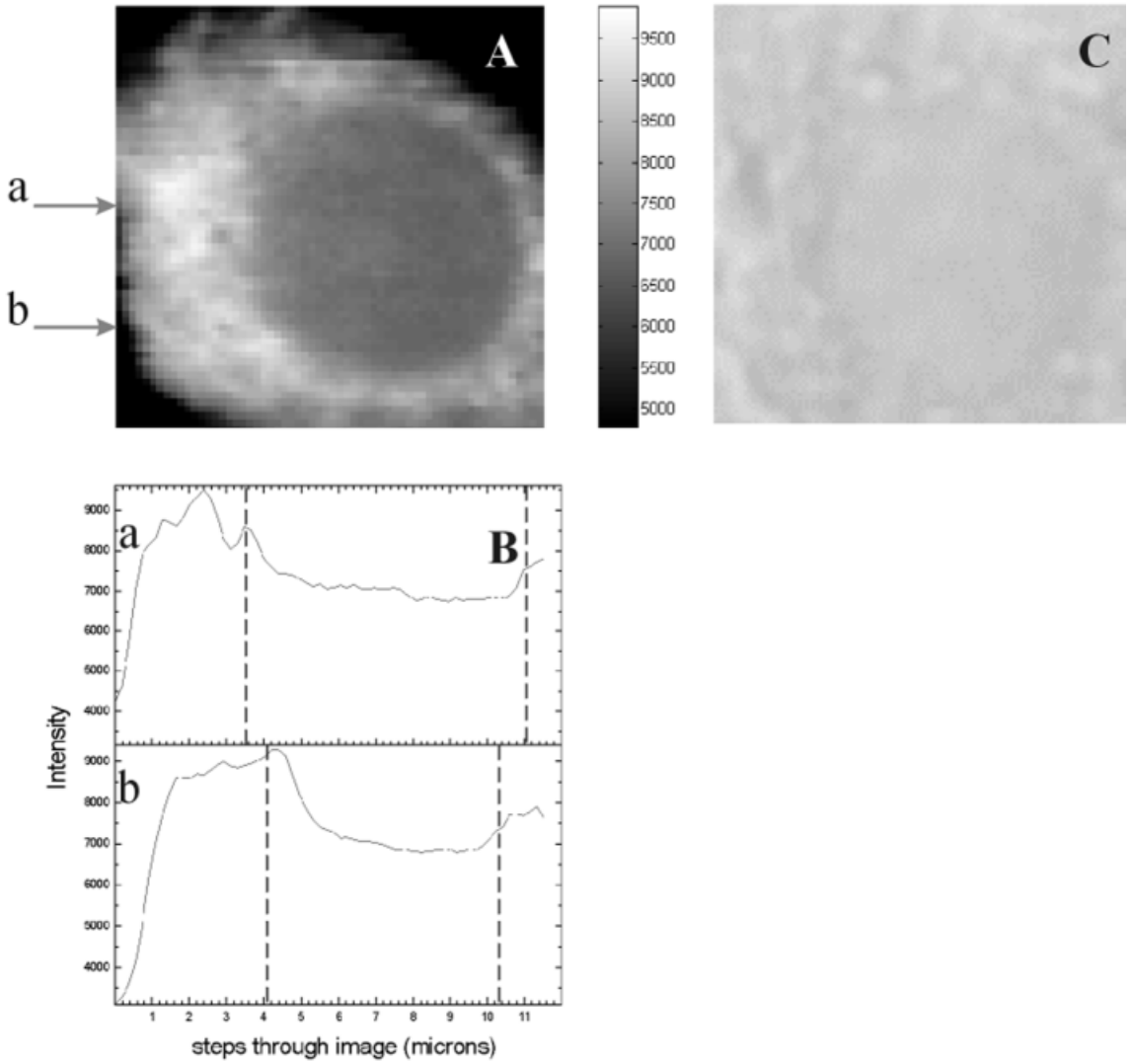

Figure 6. Raman imaging of a fixed LEC in physiological buffer. (A) A high frequency protein band consisting of 2850 cm^{-1} symmetric CH_2, 2885 cm^{-1} asymmetric CH_2, and 2935 cm^{-1} CH vibration modes; (B) two profiles through the protein image corresponding to lines a and b; (C) a transmission bright light view of the epithelial cell. The scanning area was 12 × 12 μm. The laser power was 60 mW, and the acquisition time was 1 s/step.

the epithelial cell in comparison to the epithelial cell nucleus (data not shown).

CONCLUSIONS

In this report we showed for the first time high resolution confocal Raman images of the protein distribution in single cells as obtained by nonresonant Raman scattering. Raman images of different cell types with differing levels of transcription were obtained and compared.

The Raman images of PBLs and LECs show differences in the protein distribution in the cell nuclei. In the nucleus of a mature PBL the territories of higher and lower protein intensity are clearly distinguishable. The size of some of these territories is on the order of 1 μm. On the other hand, the nucleus of the LECs appears to be more homogeneous, at least on the scale of the diffraction-limited optical resolution. Raman imaging does not require chemical labeling of compounds, but it makes use of the natural optical response of materials to laser light. In this way the technique

reports directly about material distributions (i.e., proteins in the present case) and chromatin compaction inside the nucleus. The development of Raman imaging for single cell imaging is particularly of interest where large-scale structural and organizational molecular rearrangements take place, such as in phagocytosis, apoptosis, cell differentiation, and so forth.

In this article we focused on the intense protein bands around 3000 cm^{-1} as reporter frequencies for the protein distribution. The vibrational spectrum in the fingerprint region also contains information about the nucleotide distribution inside the nucleus. This research is in progress and will be reported in a future publication. Parallel to this development, we are further improving the confocal resolution of the Raman microscope, which requires a careful analysis and correction of the point spread function in the object space of the objective, as well as in the image space where the confocal pinhole is located. This will enable a further reduction of the confocal volume but still allow for efficient photon collection from the desired measurement volume.

The authors thank Dr. E. Pels and her coworkers of the Cornea Bank in Amsterdam for making the donor eye lenses available.

REFERENCES

1. Lasch, P.; Pacifico, A.; Diem, M. Biopolym (Biospectrosc) 2002, 67, 335–338.
2. Zumbusch, A.; Holtom, G. R.; Xie, X. S. Phys Rev Lett 1999, 82, 4142–4145.
3. Puppels, G. J.; Garritsen, H. S. P.; Kummer, J. A.; Greve, J. Cytometry 1993, 14, 251–256.
4. Wood, B. R.; Tait, B.; McNauton, D. Biochim Biophys Acta 2001, 1539, 58–70.
5. Duindam, J. J.; Vrensen, G. F. J. M.; Otto, C.; Puppels, G. J.; Greve, J. J. Lipid Res 1995, 36, 1139–1146.
6. Duindam, J. J.; Vrensen, G. F. J. M.; Otto, C.; Greve, J. Invest Ophth Vis Sci 1998, 39, 94–103.
7. Feofanov, A. V.; Grichine, A. I.; Shitova, L. A.; Karmakova, T. A.; Yakubovskaya, R. I.; Egret-Charlier, M.; Vigny, P. Biophys J 2000, 78, 499–512.
8. Arzhantsev, S. Y.; Chikishev, A. Y.; Koroteev, N. I.; Greve, J.; Otto, C.; Sijtsema, N. M. J Raman Spectrosc 1999, 30, 205–208.
9. Sijtsema, N. M.; Tibbe, A. G. J.; Segers-Nolten, G. M. J.; Verhoeven, A. J.; Weening, R. S.; Greve, J.; Otto, C. Biophys J 2000, 78, 2606–2613.
10. Sijtsema, N. M.; Otto, C.; Segers-Nolten, G. M. J.; Verhoeven, A. J.; Greve, J. Biophys J 1998, 74, 3250–3255.
11. Otto, C.; Sijtsema, N. M; Greve, J. Eur Biophys J 1998, 27, 582–589.
12. Hilderbrandt, E. R.; Cozzarelli, N. R. Cell 1995, 81, 331–340.
13. Frenster, J. H.; Allfrey, V. G.; Mirsky, A. E. Proc Natl Acad Sci USA 1963, 50, 1026–1032.
14. Li, D. W.-C. Nova Acta Leopoldina 1997, NF 75/229, 81–108.
15. Shui, Y. B.; Sasaki, H.; Pan, J. H.; Hata, I.; Kojima, M.; Yamada, Y.; Hirai, K.-I.; Takahashia, N.; Sasaki, K. Exp Eye Res 2000, 71, 609–618.
16. Hightower, K. Curr Eye Res 1995, 14, 71–78.
17. Sijtsema, N. M.; Wouters, S. D.; de Grauw, C. J.; Otto, C.; Greve, J. Appl Spectrosc 1998, 52, 348–355.
18. De Grauw, C. J.; Sijtsema, N. M.; Otto, C.; Greve, J. J Microsc Oxford 1997, 188, 273–279.
19. Puppels, G. J.; van Rooijen, M.; Otto, C.; Greve, J. In Fluorescent and Luminescent Probes; Mason, W. T., Ed.; Academic: London, 1993; pp 238–258.
20. Thomas, G. J., Jr.; Prescott, B.; Olins, D. E. Science 1977, 197, 385–388.
21. Hayashi, H.; Nishimura, Y.; Katahira, M.; Tsuboi, M. Nucl Acids Res 1986, 14, 2583–2596.
22. Francastel, C.; Schubeler, D.; Martin, D. I. K.; Groudine, M. Nat Rev Mol Cell Biol 2000, 1, 137–143.
23. Mascetti, G.; Carrara, S.; Vergani, L. Cytometry 2001, 44, 113–119.
24. Kan, H.-C.; Shyy, W.; Udaykumar, H. S.; Vigneron, P.; Tran-Son-Tay, R. Ann Biomed Eng 1999, 27, 648–655.
25. Frenster, J. H. In The Cell Nucleus; Bush, H., Ed.; Academic: New York, 1974; Vols. 1–3, pp 565–580.